# Supporting Information

## Zhu et al. 10.1073/pnas.1017669108

### SI Materials and Methods

**Construction of the Structural Model of the TRPP2/PKD1 Coiled-Coil Complex.** To generate a structural model of TRPP2/PKD1 coiled-coil complex, we employed a two-step docking strategy. First, a rigid-body docking procedure was used to dock the PKD1 coiled-coil as a rigid body onto the TRPP2 coiled-coil trimer. During the docking calculation, the position and orientation of the PKD1 helix relative to the TRPP2 trimer were optimized extensively. Then, molecular dynamics (MD) simulation was used to refine the atomic details of the TRPP2/PKD1 interface.

**Stage 1: Docking PKD1 C-terminal Helix onto TRPP2 C-terminal Domain Trimer.** The docking procedure used in this stage was adapted from an iterative modular optimization (IMO) (1) procedure developed previously for refining secondary structure elements (SSEs) of homology models. The basic idea of IMO is to move SSEs as rigid bodies in torsional space (1, 2) and evaluate the sampled conformations using a statistical potential (3) in an iterative manner to search for low-energy conformations. IMO has been found to be very effective in packing helices onto protein structures in homology modeling, suggesting that it can be used to dock the PKD1 helix onto the TRPP2 coiled-coil trimer.

Fig. S10*A* illustrates a docking procedure in which the PKD1 helix was anchored to the symmetric axis of the TRPP2 trimer using a 30-glycine loop at both ends, each anchor being 10 Å away from the nearest TRPP2 atom. This procedure only allowed one predetermined packing mode, either parallel or antiparallel, defined by the N-to-C direction of the PKD1 helix relative to that of the TRPP2 trimer. In the docking, the trimer structure was treated as the protein body and the PKD1 helix as the region to be refined, just as in the standard IMO procedure. The two artificial loops served as driver regions and spatial constraint in sampling and were not involved in energy calculation. Fig. S10*B* illustrates another docking procedure used for comparison, in which the PKD1 helix was directly connected to one of the TRPP2 domains using a single, 100-glycine loop. In principle, this procedure allowed both parallel and antiparallel packing modes. In both docking procedures, the initial structure of the PKD1 helix was generated using standard geometry by setting the backbone dihedral angles $\phi$ and $\varphi$ to −60° and −45°.

Two issues that might affect docking were investigated. First, the distribution of the docked PKD1 helix in all three grooves of the TRPP2 trimer was similar, confirming that the conformational sampling was unbiased. Second, the docked PKD1 helix was relaxed using an IMO procedure where a small perturbation of 5° was applied to the backbone of two connecting loops. The resulting PKD1 conformation and energy calculated using a statistical potential based on the distance-scaled, finite, ideal-gas reference state (DFIRE) were almost unchanged, confirming that the rigid-body docking had indeed converged.

The model complexes obtained from docking were energy minimized using the program *minimize*.x in the TINKER package (4) with nonhydrogen backbone atoms fixed using a force constant of 100 kcal/mol per $\text{Å}^2$. After minimization, the lowest-energy conformation was selected for the subsequent MD simulation.

**Stage 2: Refining Model Complex Using MD Simulations.** Two MD simulation protocols were used: one involved 10 standard MD simulations and the other corresponded to a replica-exchange MD (REMD) simulation that consisted of 20 replicas. In the standard MD protocol, the model complex was first relaxed with a 200-step steepest descent energy minimization and then adapted to implicit solvent with a 100-ps restrained dynamics during which the positions of nonhydrogen atoms were fixed. In the data collection stage, ten 5-ns simulations were performed without restraints. Each of 10 simulations used a different random number to assign initial atomic velocities. In the REMD protocol, 20 simulations (replicas) were performed simultaneously at temperatures ranging from 270 to 370 K. At an interval of 5 ps, the exchange of conformations between neighboring replicas was attempted according to a Metropolis criterion except during the restrained dynamics. The data collection stage was a 5-ns simulation with an exchange rate of 0.33. Only conformations from the ten lowest-temperature replicas were used in trajectory analysis. In this study, REMD was used as an alternative MD technique to confirm the conclusions drawn from the results of standard MD simulations.

In both MD protocols, the GROMOS96 43a1 force field (5) was used in conjunction with the modified analytic generalized Born implicit solvation model (6) in simulation. The protonation state of the ionizable amino acids was set appropriate for pH 7.0 assuming standard $pK_a$s. Stochastic dynamics (SD) (7) was used with a friction coefficient of water ($\gamma_w$) that equaled 91 $ps^{-1}$ and was weighted by atomic accessibility. A time step of 2 fs was used in all simulations with the covalent bond lengths constrained by SHAKE algorithm (8). The temperature was kept at 300 K by weak coupling algorithm (9), with the relaxation time being 0.1 ps. The nonbonded interactions were calculated without cutoffs. Coordinates and energies were recorded every 1 ps.

Ten MD simulations were performed on the TRPP2 coiled-coil domain trimer using the standard MD simulation protocol described above. In each simulation, the random number used to generate initial atomic velocities was the same as in the corresponding complex simulation, except for the presence of the PKD1 coiled-coil helix in the starting structure. This approach allows us to quantitatively examine the effect of PKD1 binding on the dynamics of the TRPP2 coiled-coil trimer in solution.

**Analysis of MD Simulation Results.** A consensus-based contact analysis was used to extract the residue-residue contacts across the binding interface. A contact was defined by a cut-off distance of 7 Å between two $C_\alpha$ atoms or 6 Å between two $C_\beta$ atoms. Given the 1,000 conformations sampled in the last 1-ns simulation, a list of interfacial contacts was derived from each conformation; only those contacts that were present within >60% of the simulation time for standard MD (or 30% for REMD) were retained. These contacts were ranked according to the frequency of occurrence (FOC), defined by the number of MD simulations in which they emerged as significant contributors to the complex conformation.

A structure clustering algorithm was adapted to identify a small set of conformations that could best represent the conformational space sampled. The basic idea was to iteratively group the conformations into clusters and then select energetically the most favorable conformation as the cluster center. This algorithm has been successfully applied to a number of studies. In this work the conformations sampled in the last 1-ns simulation were collected from all 10 MD runs for clustering and the clustering cut-off was set to 3.5 Å. The representative conformations of top 20 clusters were further analyzed in detail.

**Constructs and Cloning.** All mutations were introduced into the WT constructs by PCR and the mutation sites were confirmed by sequencing. Experiments involving protein fragments were done

using the human TRPP2 [National Center for Biotechnology Information (NCBI) accession no. U50928] and PKD1 (NCBI accession no. L39891), whereas experiments involving full-length proteins were done using the human TRPP2 and mouse PKD1 (mPKD1, NCBI accession no. NM_013630).

For constructs used in pull-down and disulfide bond analysis experiments, PCR-generated WT or mutant TRPP2 C-terminal fragments were cloned into pET28a(+) (Novagen) vector. A 22-aa peptide (MGSSHHHHHHSSGLVPRGSHM) containing a $His_6$ tag was introduced at the N terminus of the TRPP2 fragments. The coiled-coil domain fragments of WT or mutant human PKD1 were cloned into a modified pCDFduet-1 (Novagen) vector containing a maltose binding protein (MBP) cDNA; thus the PKD1 fragments all contained an MBP tag on the N terminus.

Full-length human TRPP2 and mouse PKD1 were used in coimmunoprecipitation (coIP) and immunofluorescence experiments. An HA tag was added to the N terminus of TRPP2, and the construct was cloned into the pCDNA3.1(−) vector (Invitrogen). The signal peptide (M1–A23) of mouse PKD1 was replaced by a Ig k-chain leader sequence (METDTLLLWVLLLWVPGSTGD) and a FLAG tag was added immediately after this sequence. This construct was cloned into the pIRESpuro2 vector (Clontech).

For constructs used in the total internal reflection fluorescence (TIRF) imaging experiments, human TRPP2 and mouse PKD1 cDNA were cloned into a modified pGEMHE vector containing the EGFP or mCherry cDNA, respectively, in the multiple cloning sites, with a flexible linker (SRGTSGGSGGSRGSGGSGG) in between. The final constructs were TRPP2–SRGTSGGSGGSRGSGGSGG–EGFP and mPKD1–SRGTSGGSGGSRGSGGSGG–mCherry.

**Expression of Protein Fragments, Pull-Down, and Chromatography.** $His_6$-tagged TRPP2 fragments and MBP-tagged PKD1 fragments were coexpressed in the *Escherichia coli* strain Rosetta 2(DE3) (Novagen), and purified with Ni-nitrilotriacetate (NTA) His•-Bind superflow resins (Novagen) by following the manufacturer's protocol. The bacteria lysis solution contained 50 mM Tri·HCl, 250 mM NaCl, 7 mM β-mercaptoethanol (β-ME) and 2.5% glycerol (pH 7.8). The protein complex was eluted from the Ni-NTA His•Bind beads with 250 mM imidazole in the lysis solution and analyzed by SDS-PAGE. More details were described previously in ref. 10.

To determine the oligomerization state of the PKD1 coiled-coil, MBP-tagged PKD1_S4212–R4248 fragments were expressed in *E. coli* as described above. The cell lysates were incubated with the MBP-binding amylose resin (New England Biolabs) at 4 °C for 2 h. The beads were centrifuged at 2,000 rpm for 1 min, collected and washed with 20 vol of the above lysis solution. Bound protein was then eluted with the same lysis solution containing 20 mM maltose. This protein was further purified with a Superose 12-gel filtration column (GE Healthcare).

**Light-Scattering Measurements.** Gel filtration-purified MBP–PKD1_S4212–R4248 fragments from above were run through another gel filtration column protein KW-802.5 (Shodex) with a solution containing 200 mM NaCl and 100 mM Tris·HCl (pH 7.5). Eluates were examined by static light-scattering (Wyatt Technology).

**Disulfide Bond Analysis.** WT and mutant TRPP2/PKD1 coiled-coil complexes were expressed and purified with Ni-NTA beads (see above). Proteins eluted from the beads were further incubated with the MBP-binding amylose resin (New England Biolabs) and then collected as above. Beads were resuspended and washed with 20 vol of the above lysis solution without β-ME. The protein complexes were then eluted from the beads with the same solution contains 20 mM maltose. Protein samples were mixed with either unreduced sample buffer (3X SDS blue loading buffer, New England Biolabs), or reduced sample buffer (3X SDS sample buffer with 100 mM DTT and 5% β-ME added). Samples were boiled for 3 min and analyzed by SDS-PAGE with NuPAGE novex 4–12% Bis-Tris gels (Invitrogen).

**Coimmunoprecipitation.** HEK 293T cell lines that stably express either FLAG-tagged mouse PKD1 or HA-tagged TRPP2 were used in the coIP experiments. The transiently expressed cDNA was transfected into the stable cells with Lipofectamine 2000 (Invitrogen). Monoclonal antiFLAG antibody (M2) coated beads (Sigma) were used to IP the proteins from cell lysates prepared 36–40 h after transfection. The bound proteins were eluted with 1X SDS sample loading buffer. Details of stable cell line generation, cell culture, transfection, cell lysis, and IP were described previously (10). Samples were analyzed by SDS-PAGE and Western blotting.

**SDS-PAGE and Western Blotting.** SDS-PAGE was performed in Tris-glycine buffer under reducing condition with 10 or 15% acrylamide gel for pull-down experiments; or in MOPS buffer under nonreducing condition with NuPAGE novex 4–12% Bis-Tris gels (Invitrogen) for disulfide bond analysis experiments. Precision Plus Protein All Blue Standards (BioRad) was used as molecular mass markers. Gel pictures were taken with a Kodak gel imaging system.

Western blotting was done with the One-Step Western Kit (GenScript). The primary antibodies used were mouse monoclonal antiHA antibody (Covance) and mouse monoclonal anti-FLAG antibody (Sigma). The secondary antibody used was Alexa Fluor 680 goat anti-mouse IgG (Invitrogen). Membranes were scanned with the Odyssey Infrared Imaging System (Li-COR).

For both pull-down and coIP experiments, the intensity of the protein bands was analyzed with the software ImageJ, and the effects of the mutations were quantified by calculating the ratio of the band intensity of the following two protein pairs: MBP–PKD1 fragment : $His_6$–TRPP2 fragment (for SDS-PAGE gels in pull-down experiments) and full-length HA–TRPP2 : full – length FLAG–PKD1 (for Western blotting in coIP experiments).

**Surface Channel Analysis with Immunofluorescence.** HEK 293T cells were transfected with appropriate DNA combinations with Lipofectamine 2000 (Invitrogen) and incubated for 36 h. Cells were washed twice with PBS solution and then fixed with 4% paraformaldehyde in PBS for 15 min. After a 5-min wash with PBS three times, cells were either *permeabilized* with 0.25% Triton X-100 for 20 min followed by three 5-min washes or processed similarly but without Triton X-100. Subsequently, cells were blocked with 1% goat serum in PBS for 1 h and incubated with the monoclonal antiFLAG (Sigma) antibody in the same blocking solution at 4 °C overnight. After three 10-min washes with PBS, the cells were incubated with fluorescein (FITC)-conjugated goat anti-mouse IgG and 1% goat serum in PBS for 1 h at room temperature. After another three 10-min washes with PBS, cells were mounted on slides and imaged with an Olympus confocal microscope.

**Surface Channel Analysis with TIRF Microscopy.** The detailed methods were described previously (10, 11). In brief, 24–48 h after injection of in vitro transcribed cRNAs, *Xenopus* oocytes were treated to enable a close contact with the coverslip. A 488-nm Argon laser was used to excite EGFP and a 593-nm DPSS laser was used to excite mCherry. Spots that exhibited both EGFP and mCherry fluorescence were considered as TRPP2/PKD1 complexes.

1. Zhu J, Xie L, Honig B (2006) Structural refinement of protein segments containing secondary structure elements: Local sampling, knowledge-based potentials, and clustering. *Proteins Struct Funct Bioinf* 65:463–479
2. Canutescu AA, Dunbrack RL (2003) Cyclic coordinate descent: A robotics algorithm for protein loop closure. *Protein Sci* 12:963–972
3. Zhou HY, Zhou YQ (2002) Distance-scaled, finite ideal-gas reference state improves structure-derived potentials of mean force for structure selection and stability prediction. *Protein Sci* 11:2714–2726
4. Ponder JW (1999) *TINKER-software tools for molecular design* (Washington University, St. Louis, MO), Version 3.7.
5. van Gunsteren WFB, et al. (1996) Groningen Molecular Simulation (GROMOS) System. University of Groningen; the Netherlands, ETH Zurich; Switzerland), Version GROMOS96.
6. Zhu J, Alexov E, Honig B (2005) Comparative study of generalized born models: Born radii and peptide folding. *J Phys Chem B* 109:3008–3022
7. van Gunsteren WF, Berendsen HJC, Rullmann JAC (1981) Stochastic dynamics for molecules with constraints Brownian dynamics of normal-alkanes. *Mol Phys* 44:69–95
8. Ryckaert JP, Ciccotti G, Berendsen HJC (1977) Numerical-integration of cartesian equations of motion of a system with constraints—molecular-dynamics of n-alkanes. *J Comput Phys* 23:327–341
9. Berendsen HJC, Postma JPM, Vangunsteren WF, Dinola A, Haak JR (1984) Molecular-dynamics with coupling to an external bath. *J Chem Phys* 81:3684–3690
10. Yu Y, et al. (2009) Structural and molecular basis of the assembly of the TRPP2/PKD1 complex. *Proc Natl Acad Sci USA* 106:11558–11563
11. Ulbrich MH, Isacoff EY (2007) Subunit counting in membrane-bound proteins. *Nat Methods* 4:319–321
12. Jones DT (1999) Protein secondary structure prediction based on position-specific scoring matrices. *J Mol Biol* 292:195–202


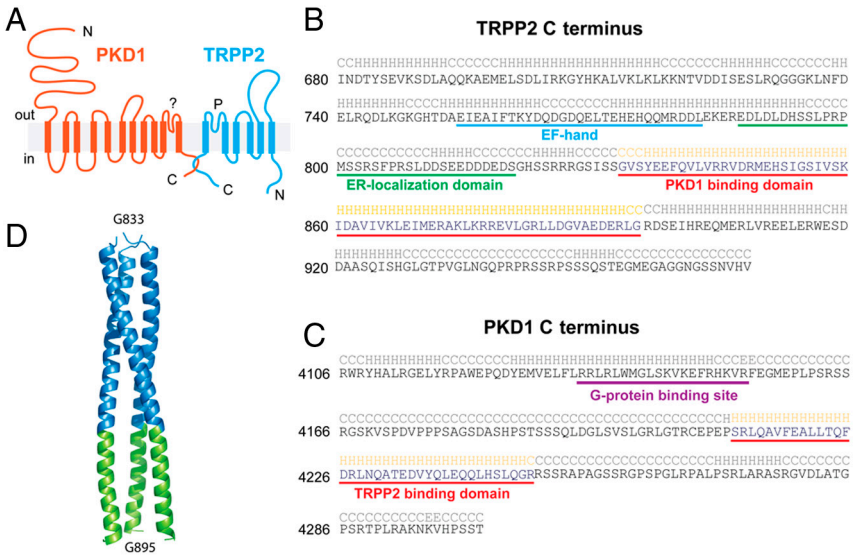


**Fig. S1.** Molecular and structural information about the TRPP2 and PKD1 C termini. (*A*) Putative transmembrane topology of PKD1 and TRPP2. The cytoplasmic C termini of both subunits interact directly. It remains to be determined whether PKD1 contains a pore-forming loop between its last two transmembrane segments or elsewhere. (*B* and *C*) Amino acid sequence (*Bottom*) and secondary structure predicted by PSIPRED (12) (*Top*) of the C termini of TRPP2 and PKD1, with C and H denoting random coils and α-helices, respectively. (*D*) X-ray crystal structure of the TRPP2 C-terminal coiled-coil trimer determined at a resolution of 1.9 Å (10).

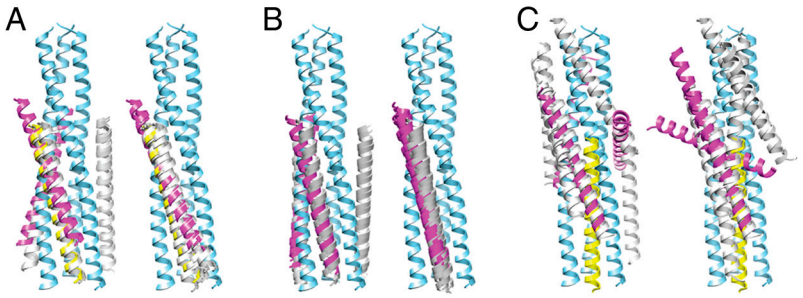


**Fig. S2.** Superposition of 10 docking models of the TRPP2/PKD1 coiled-coil domain complex generated by different procedures. (*A*) Parallel docking. (*B*) Antiparallel docking. (*C*) Random docking. For each docking condition, the original docking conformations without considering the symmetry of the TRPP2 coiled-coil trimer are shown on the left and the docking conformations after fitting into a single groove are shown on the right. The TRPP2 coiled-coils are colored in light blue. In *A* and *B*, the 10 conformations of the PKD1 coiled-coil are colored according to the energy and rmsd analysis in Fig. 1: Eight lower-energy models (7, 2, 5, 4, 8, 9, 1, and 6) are gray and two higher-energy models (3 and 10) are magenta. Conformation 4 in parallel docking is colored in yellow (*A*). In *C*, seven parallel packing conformations, which on average have lower DFIRE energies, are colored gray expect for 3, which is colored yellow as it is similar to 4 in parallel docking and has the lowest energy. The two antiparallel packing conformations are colored magenta.

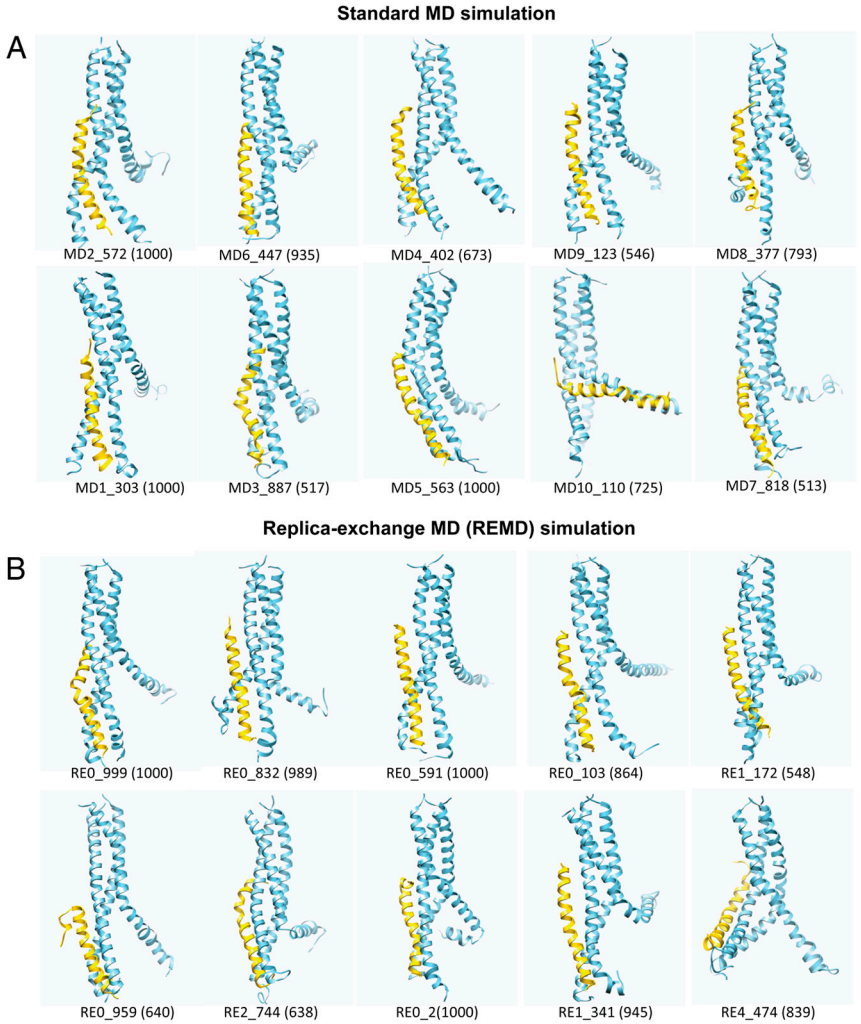


**Fig. S3.** Representative conformations of the TRPP2/PKD1 coiled-coil complex. The conformations were selected from the top 10 lowest-energy clusters obtained from standard MD simulations (*A*) and REMD simulations (*B*). Each conformer is uniquely designated by the index of the MD or replica run (i.e., MDx or REx), the snapshot index, and the number of total conformations in that particular cluster (in parentheses). TRPP2 and PKD1 coiled-coils are shown in light blue and gold, respectively.

The conformations sampled in the last 1-ns simulation, from either 10 standard MD runs or 10 low-temperature REMD replicas, were combined into one dataset for clustering analysis. Notably, the representative conformations in *A* were obtained from different MD runs, whereas 6 out of the 10 representative conformations in *B* were obtained from the lowest-temperature replica. This difference was due to the communication between replicas in the REMD simulation, where conformations in the neighboring replicas could be exchanged based on the probability calculated from the Metropolis criterion. Thus, the trajectory of each REMD replica contained conformations from other replicas and the lowest-temperature replica tended to collect more low-energy conformations from other replicas, which very often became the centers of clusters in the clustering analysis. In contrast, standard MD simulations were totally independent of each other and represented different sampling pathways in the conformational space.

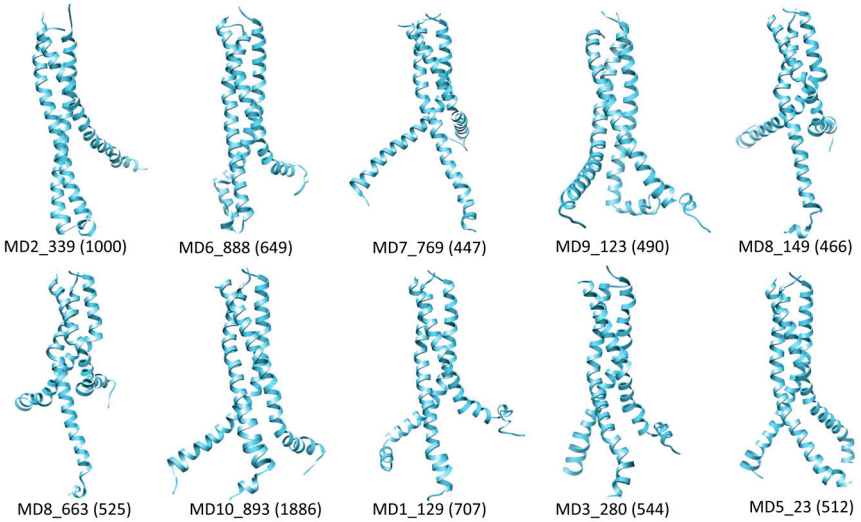


**Fig. S4.** Representative conformations of the TRPP2 coiled-coil domain trimer. The conformations sampled in the last 1-ns simulation from 10 standard MD simulations were combined into one dataset for clustering analysis. The conformations were selected from the top 10 lowest-energy clusters with the requirement that each cluster contained at least 400 conformations. Note that 400 instead of 500 was used here due to a more dispersed distribution of the TRPP2 trimer conformations caused by the flexibility of its C-terminal regions. The conformer index for the trimer is formatted in the same way as for the TRPP2/PKD1 complex in Fig. S3. The TRPP2 coiled-coils are colored light blue.

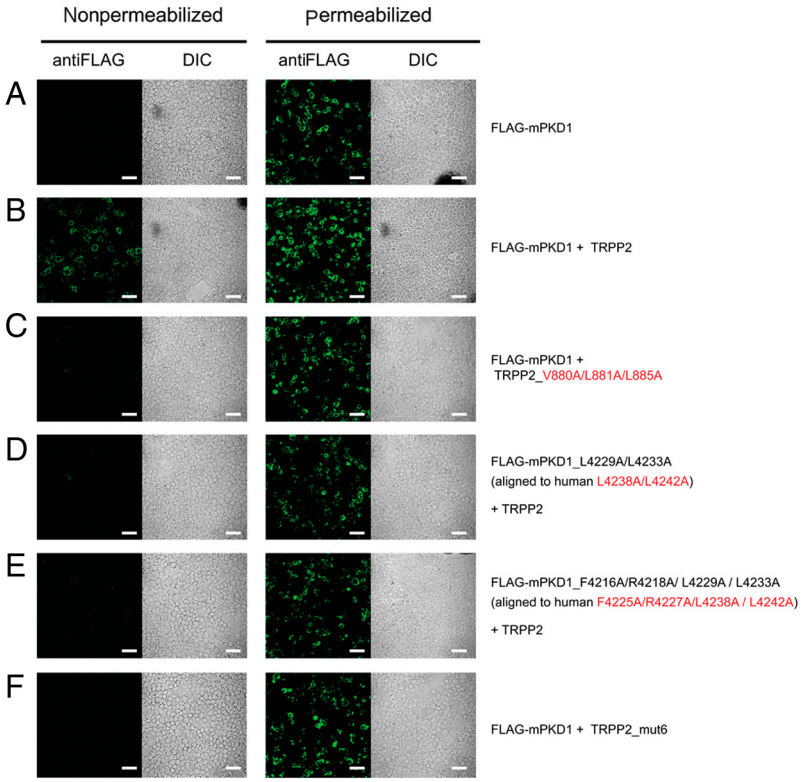


**Fig. S5.** Disruption of the TRPP2/PKD1 coiled-coil complex abolishes surface expression of the full-length TRPP2/PKD1 complex in HEK 293T cells. HEK 293T cells were transfected with the indicated combinations of constructs. FLAG-tagged mouse PKD1 (FLAG–mPKD1) was visualized by confocol microscopy after being stained with an antiFLAG primary antibody and FITC-conjugated secondary antibody (green). Total expression of PKD1 was examined under the permeabilized condition and surface expression of PKD1 was examined under the nonpermeabilized condition. Differential interference contrast (DIC) images show the bright-field view of all the cells. In the permeabilized condition, numerous cells were stained for each combination of constructs, indicating that the PKD1 protein was made; however, in the nonpermeabilized condition, stained cells were observed only with the cotransfection of WT FLAG–mPKD1 and WT TRPP2 (*B*). PKD1 did not reach the plasma membrane on its own (*A*) but did so when coexpressed with WT TRPP2 (*B*). Disrupting the TRPP2/PKD1 coiled-coil interaction by mutating key interface residues on either TRPP2 (*C*) or PKD1 (*D* and *E*) abolished PKD1 surface expression. As expected, PKD1 surface expression was also abolished when PKD1 was coexpressed with a mutant TRPP2 (TRPP2_mut6) which bears six alanine mutations in the TRPP2 coiled-coil and cannot associate with PKD1 (*F*) (10). Scale bar: 50 μm.

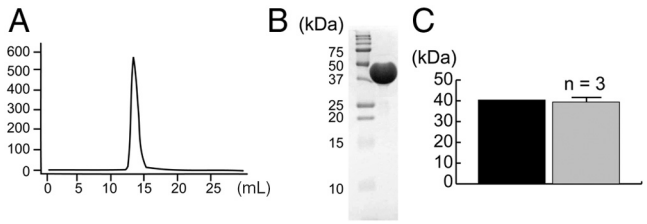


**Fig. S6.** The PKD1 coiled-coil domain is a monomer. (*A*) Gel filtration profile of an MBP-tagged PKD1 coiled-coil domain fragment (MBP–PKD1_S4212–R4248), showing a single sharp peak. (*B*) In SDS-PAGE, MBP–PKD1_S4212–R4248 migrates as a single band with a molecular mass equal to a monomer. (*C*) The calculated molecular mass of monomeric MBP–PKD1_S4212–R4248 is 40.4 kDa (black bar). The experimentally measured (by static light-scattering) molecular mass of MBP–PKD1_S4212–R4248 is 39.4 ± 0.8 (mean ± SD.) (gray bar), indicating that MBP–PKD1_S4212–R4248 exists as a monomer in solution.

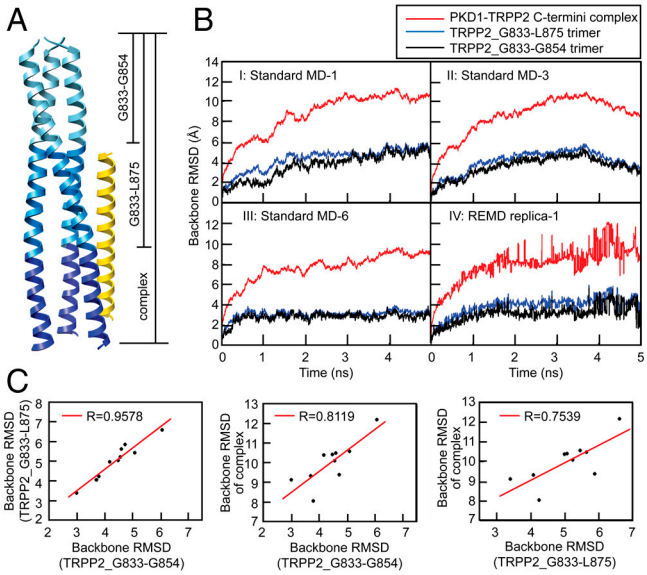


**Fig. S7.** Root mean square deviation analysis of the backbone of the TRPP2/PKD1 coiled-coil complex. (*A*) Based on the TRPP2 sequence, three sets of atoms were specified in the rmsd calculation: the first corresponding to the N-terminal 22 aa from G833 to G854, a secondary structure breaker; the second from G833 to L875, preceding a highly charged KRRE region; and the last comprising the entire TRPP2/PKD1 complex. (*B*) Plots of the rmsd as a function of simulation time for three independent MD runs (1, 3, and 6), as examples, and for the lowest-temperature replica in the REMD simulation. As can be seen, the conformational space was being explored along different paths in the three exemplary MD runs. However, the three rmsd measures in each MD run, although differ in numbers, appear to be correlated to one another. (*C*) To examine this possibility, we calculated the average rmsd of the last 1-ns simulation for all 10 MD runs and then calculated the correlation between any two measures. The correlation coefficient ranged from 0.754 to 0.958, suggesting that the conformational change of the small TRPP2 N-terminal segments (3 × 22 residues) orchestrates the conformational change of the entire complex [3 × 65 (TRPP2) +37 (PKD1) residues]. The 10 MD simulations of the TRPP2 coiled-coil trimer yielded similar results (Fig. S8).

Frequent exchange between replicas in REMD simulation was also plotted (*B*, *iv*). The three rmsd measures behaved similarly as they did in the standard MD simulations, leading to essentially the same conclusion as above.

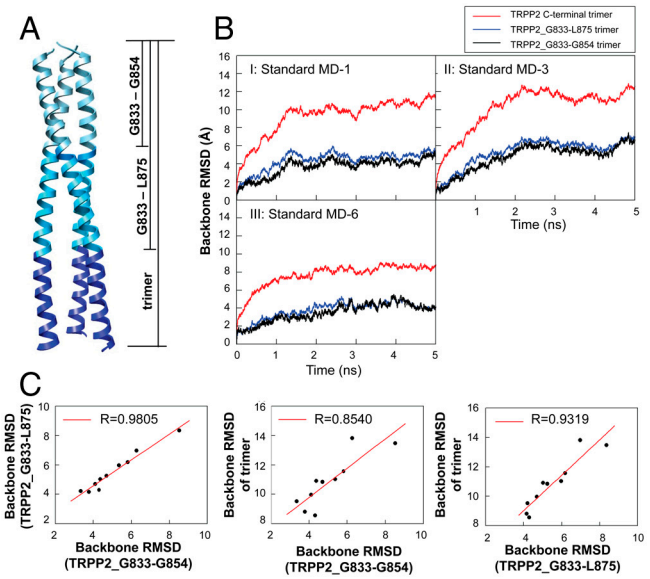


**Fig. S8.** Root mean square deviation analysis of the backbone of the TRPP2 coiled-coil domain trimer. (*A*) Based on the TRPP2 sequence, three sets of atoms were specified in the rmsd calculation: the first corresponding to the N-terminal 22 aa from G833 to G854, a secondary structure breaker; the second from G833 to L875, preceding a highly charged KRRE region; and the last comprising the entire trimer structure. (*B*) Plots of the rmsd as a function of simulation time for three independent MD runs: 1, 3, and 6. Similar to the complex simulations, the conformational space was being explored along different paths in the three examplar MD runs. (*C*) The three rmsd measures in each MD run are correlated to one another. We calculated the average rmsd of the last 1-ns simulation for all 10 MD runs and then calculated the correlation between any two measures. The correlation coefficient ranged from 0.854 to 0.981, suggesting that the conformational change of the trimer is guided by the N-terminal segments ($3 \times 22$ residues). This finding is consistent with the observation for the TRPP2/PKD1 coiled-coil complex (Fig. S7).

Based on these results, we conclude that the N-terminal portion of the TRPP2 trimer that is tightly bundled together determines the dynamics of the entire trimer or the TRPP2/PKD1 complex. We then compared the average rmsd values from the TRPP2 trimer alone and TRPP2/PKD1 complex simulations using the paired Student's *t*-test, which offers a quantitative measure of to what extent the binding of the PKD1 helix affects the dynamics of the TRPP2 coiled-coil trimer. The two-tailed P value was 0.291, indicating that the effect of PKD1 binding is statistically not significant. Taken together, it seems that at the fragment level the TRPP2 trimer plays a central role in the physical association of TRPP2 and PKD1, and that a small conformational change originating from the N-terminal portion of the trimer propagates through the entire trimer or complex while being amplified.

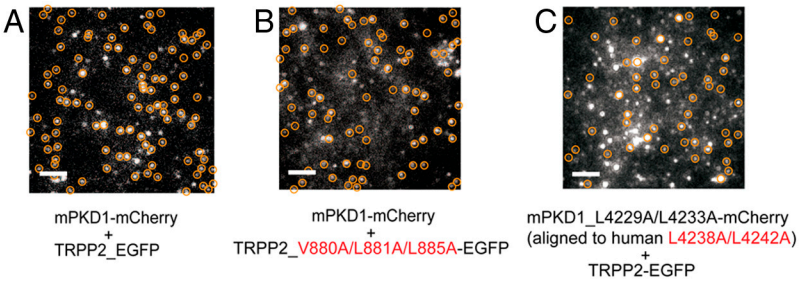


**Fig. S9.** Disruption of the TRPP2/PKD1 coiled-coil complex does not completely abolish the assembly of the full-length TRPP2/PKD1 complex in *Xenopus* oocytes. TIRF microscopy was used to visualize mPKD1 and EGFP-tagged TRPP2 (10). (*A*, *B*, *C*) TIRF image of mCherry fluorescence from oocytes expressing the indicated combinations of constructs. Scale bar: 2 μm. Spots circled in orange were immobile and exhibited mCherry and EGFP dual fluorescence (EGFP fluorescence image not shown), representing the TRPP2/mPKD1 complex. Uncircled fluorescent spots, including some very bright spots in *C*, showed only mCherry fluorescence. The lack of EGFP fluorescence in these spots could be caused by movement of these spots in between mCherry and EGFP excitations or in-plasma membrane dissociation of mPKD1 and TRPP2. It is of interest to note that the L4229A/L4233A mutation in mPKD1 appears to increase the relative number of mCherry fluorescence-alone spots, consistent with a weakened association between mPKD1_ L4229A/L4233A and TRPP2.

In agreement with our previous study (10), mPKD1 reached the plasma membrane of *Xenopus* oocytes when it was coexpressed and coassembled with TRPP2 (*A*). When TRPP2_V880A/L881A/L885A–EGFP was coexpressed with mPKD1–mCherry, spots with dual mCherry and EGFP fluorescence (not shown) were observed on the surface membrane (*B*), indicating that this mutant TRPP2 could still associate with PKD1 to form a complex. Similarly, mPKD1_L4229A/L4233A–mCherry (corresponding to human L4238A/L4242A) was also still able to assemble with TRPP2–EGFP and to be expressed on the surface membrane (*C*). It should be noted, however, that this imaging experiment was not quantitative due to many variables, including the amount of cRNA injected, the expression time, and the oocyte location where imaging was performed. Even a significant reduction in the surface expression of the TRPP2/PKD1 complex might not have been detected by this method. Thus, these results do not contradict the conclusion that the TRPP2/PKD1 coiled-coil interaction is critical for the assembly of the TRPP2/PKD1 complex. They do, however, suggest that other regions of TRPP2 and PKD1 also contribute to the assembly of the full-length TRPP2/PKD1 complex.

The reasons for the discrepancy between the results from oocytes (this figure) and HEK 293T cells (Fig. 5 *D*–*G* and Fig. S5) are unclear. One possibility is that HEK 293T cells have a more strict quality-control machinery than oocytes do. Another possibility is that oocytes contain an endogenous protein that can chaperone a small fraction of the TRPP2/PKD1 complex to the plasma membrane.

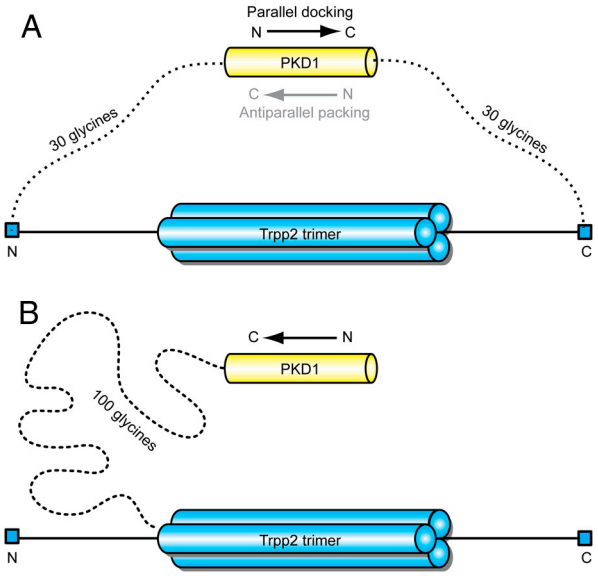


**Fig. S10.** Docking strategies. (*A*) Two docking procedures in which the PKD1 helix is anchored either parallelly (black) or antiparallelly (gray) to the TRPP2 coiled-coil domain trimer with two 30-glycine linkers in a predefined packing mode. (*B*) A random docking procedure in which the PKD1 helix is anchored to the N terminus of the TRPP2 coiled-coil domain trimer via a single 100-glycine linker, thus allowing the PKD1 helix to be packed in either the parallel or antiparallel orientation.

**Table S1. Selected residue-residue contacts extracted from the last 1 ns of MD simulations**

| Cα-based contacts | | | | | Cβ-based contacts | | | | |
|---|---|---|---|---|---|---|---|---|---|
| PKD1 | TRPP2 | $\langle r_{C\alpha\text{-}C\alpha}\rangle$ | ⟨FOC⟩ | $N_{sim}$ | PKD1 | TRPP2 | $\langle r_{C\beta\text{-}C\beta}\rangle$ | ⟨FOC⟩ | $N_{sim}$ |
| Standard MD simulation protocol | | | | | | | | | |
| Q4240 | V880 | 6.0 | 0.95 | 7 | Q4240 | V880 | 5 | 0.94 | 8 |
| Y4236 | R877 | 5.9 | 0.89 | 7 | Y4236 | K876 | 4.7 | 0.94 | 8 |
| N4229 | I869 | 6.4 | 0.83 | 7 | F4225 | V865 | 5.3 | 0.83 | 7 |
| L4242 | L885 | 6.1 | 0.88 | 6 | E4239 | R877 | 5.3 | 0.86 | 6 |
| Q4246 | R893 | 5.4 | 0.86 | 5 | L4238 | L881 | 4.1 | 0.99 | 5 |
| L4238 | L881 | 6.3 | 0.92 | 5 | L4228 | L869 | 5.0 | 0.87 | 5 |
| Q4240 | R877 | 5.6 | 0.98 | 5 | N4229 | L869 | 5.3 | 0.80 | 4 |
| E4239 | R877 | 6.4 | 0.78 | 5 | V4217 | I864 | 5.2 | 0.96 | 4 |
| Y4236 | K876 | 6.4 | 0.88 | 5 | R4213 | D861 | 5.2 | 0.73 | 4 |
| V4217 | I864 | 6.3 | 0.89 | 4 | V4217 | I860 | 5.3 | 0.89 | 4 |
| R4213 | S855 | 6.2 | 0.83 | 4 | Q4246 | L894 | 5.1 | 0.74 | 3 |
| Q4246 | L894 | 5.4 | 0.99 | 3 | Q4246 | V888 | 4.8 | 0.96 | 3 |
| Q4246 | V888 | 5.6 | 0.91 | 3 | L4245 | V888 | 5.0 | 0.88 | 3 |
| L4245 | V888 | 6.2 | 0.77 | 3 | Y4236 | V880 | 5.0 | 0.89 | 3 |
| L4221 | V863 | 6.2 | 0.94 | 3 | F4225 | I869 | 5.3 | 0.80 | 3 |
| R4213 | S858 | 5.9 | 0.84 | 3 | Q4246 | R893 | 4.6 | 0.84 | 2 |
| Q4246 | E892 | 6.2 | 0.89 | 2 | H4243 | R883 | 5.4 | 0.80 | 2 |
| Y4236 | V880 | 6.3 | 0.92 | 2 | D4234 | R878 | 5.3 | 0.84 | 2 |
| D4234 | R878 | 6.5 | 0.71 | 2 | R4227 | E871 | 4.9 | 0.90 | 2 |
| L4228 | I869 | 6.4 | 0.96 | 2 | Q4224 | E871 | 5.3 | 0.80 | 2 |
| F4225 | I869 | 6.5 | 0.81 | 2 | Q4224 | K866 | 5.5 | 0.81 | 2 |
| Q4224 | E868 | 6.5 | 0.81 | 2 | L4221 | V863 | 5.4 | 0.75 | 2 |
| F4225 | V865 | 6.6 | 0.69 | 2 | R4213 | S858 | 5.4 | 0.78 | 2 |
| R4213 | D861 | 5.9 | 0.81 | 2 | L4214 | V857 | 5.3 | 0.70 | 2 |
| L4214 | V857 | 6.3 | 0.79 | 2 | L4245 | L885 | 4.5 | 0.99 | 1 |
| L4245 | L894 | 6.0 | 0.91 | 1 | L4242 | L885 | 4.2 | 0.97 | 1 |
| L4245 | L885 | 5.8 | 0.99 | 1 | Q4246 | L884 | 5.3 | 0.61 | 1 |
| Q4246 | L884 | 6.1 | 0.69 | 1 | | | | | |
| Replica-exchange MD simulation protocol | | | | | | | | | |
| Q4246 | L894 | 5.5 | 0.45 | 9 | L4238 | L881 | 4.2 | 0.90 | 9 |
| Q4246 | R893 | 5.2 | 0.46 | 9 | H4243 | V880 | 4.8 | 0.62 | 9 |
| L4242 | L885 | 6.2 | 0.68 | 9 | Q4240 | V880 | 5.1 | 0.71 | 9 |
| L4238 | L881 | 6.3 | 0.80 | 9 | D4234 | R878 | 5.2 | 0.58 | 9 |
| N4229 | I869 | 6.3 | 0.56 | 9 | Y4236 | K876 | 4.4 | 0.70 | 9 |
| Q4240 | V880 | 6.0 | 0.73 | 8 | Y4236 | R877 | 4.8 | 0.60 | 8 |
| D4234 | R878 | 6.5 | 0.47 | 8 | N4229 | I869 | 5.3 | 0.51 | 8 |
| Y4236 | R877 | 5.6 | 0.71 | 8 | L4228 | I869 | 5.3 | 0.43 | 8 |
| Y4236 | K876 | 6.4 | 0.59 | 8 | E4239 | R877 | 5.4 | 0.49 | 5 |
| E4239 | R877 | 6.6 | 0.39 | 3 | Q4241 | L885 | 5.6 | 0.37 | 4 |
| Q4240 | R877 | 6.2 | 0.38 | 2 | L4242 | L885 | 5.4 | 0.38 | 3 |
| L4228 | L875 | 6.3 | 0.38 | 1 | R4213 | H851 | 5.2 | 0.36 | 3 |
| | | | | | Q4246 | R893 | 4.8 | 0.40 | 2 |
| | | | | | L4245 | V888 | 5.1 | 0.38 | 2 |
| | | | | | H4243 | R883 | 5.3 | 0.38 | 2 |
| | | | | | Y4236 | V880 | 5.0 | 0.42 | 2 |
| | | | | | F4225 | V865 | 5.3 | 0.40 | 2 |
| | | | | | L4242 | L884 | 5.7 | 0.37 | 1 |
| | | | | | R4213 | S855 | 4.7 | 0.37 | 1 |

One thousand conformations sampled in the last 1-ns simulation of 10 standard MD simulations and of 10 lowest-temperature replicas from the REMD simulation were subjected to the contact analysis. A distance cut-off of 7.0 and 6.0 Å was used for $C_\alpha$-$C_\alpha$ and $C_\beta$-$C_\beta$ contact analysis, respectively. For a residue-residue contact, if the frequency of occurrence (FOC) was higher than 0.6 in the case of standard MD simulation or 0.35 in the case of REMD simulation, it was considered a stable contact. The columns in each subtable list the contact residue in PKD1, the contact residue in TRPP2, the average contact distance, the average FOC, and the total number of simulations ($N_{sim}$) in which this contact was observed.

## Other Supporting Information Files

Dataset S1 (TXT)

Dataset S2 (TXT)